Journal of Harbin Engineering University
ISSN: 1006-7043
Vol 44 No. 11
November 2023

Solidification Behavior of Liquid Metal in Mould Cavity with and Without Jet Pouring System in Continuous Casting

[1]Mr. Satyendra Upadhyaya, [2] Dr. Nagendra Prasad Yadav
[1]Research Scholar, Bundelkhand Institute of Engineering and Technology, Jhansi, (U.P.), India,
[2]Professor, Bundelkhand Institute of Engineering and Technology, Jhansi, (U.P.), India,

Abstract
This paper spotlights on the solidification behavior of a continuous casting process with and without a jet-pouring system in a rectangular steel billet with a square cross section. The parametric exploration of the solidification process during continuous casting is carried out by the solidification-melting model integrated with the volume of fluid (VOF) model. The simulation was done with the computational package ANSYS (Version 19R3). The solidification behavior is evaluated by estimating the temperature, velocity, and liquid fraction inside the mould at different pouring temperatures and different inlet velocities with and without jets. The uniformity of velocity and temperature profiles inside the cavity are changed with an increase in inlet velocity at a constant pouring temperature, with and without a jet pouring system. The uniform temperature and velocity distribution inside the mould suggested uniform solidification propagation, which was justified by the liquid fraction profile inside the mould. The solidification is propagated from the bottom in the jet system, and it is propagated from the wall side in the absence of the jet system. The better solidification behavior is observed at 0.177 m/s inlet velocity and 1803 K pouring temperature at 1118 K constant wall temperature in the absence of a jet, and in the jet pouring system, better solidification is observed at 10 times higher velocity at the same temperature.
Keywords Solidification, Pouring, Temperature, Liquid Fraction, Volume of Fluid

1 Introduction

The manufacturing of any product to the desired shape and size has been compelled by the current worldwide economic calamity. Therefore, manufacturers are forced to produce a better product with a lower cast. In view of that, the processing of the molten metal requires advancements in the casting process. The casting processes necessitate the combination of heat transfer with phage change and fluid flow at the macroscopic level. The flourishing casting operation needs an understanding of moulds and pattern design, liquefied metal melting, pouring, solidification, and additional cooling to the surrounding temperature. The superior qualities of blemish-free casting can be achieved by a suitable melting of the metal and a pouring system with solidification. These are crucial. Consequently, the appropriate gating systems are needed to recuperate the
difficulties during the pouring of molten into the mold cavity. The pouring temperature and pouring rate are the two main concerns during pouring take place. The structural character of cast material and the control of its properties are decided by the solidification process. Hence, experimental as well as computational studies are needed to develop a better casting system with defect-free casting.

The researchers are dedicated to progression enhancement for the manufacture of high-prominence casting goods at low costs. Continuous casting is one of the significant casting processes that make overmolten metal into a solid on a permanent basis and consists of a diversity of momentous manufacturing processes. It is a normally well-organized means to solidify large volumes of metal into simple forms for ensuing processing. The sooner liquid metal
solidifies in the case of the reverse flow condition than in the secondary flow direction [1]. Swaminathan and Voller [2] have analyzed the solidification systems with the common implicit source-based enthalpy method. It is used for the option of enthalpy temperature relationship and the proficient examination of metallurgical solidification trends. Swaminathan and Voller [3] have approximated the convective flux with the volume of fluid method. The complex phase change process associated with the modeling of general casting exertion involves filling and additional

coupled phenomena (i.e., solidification and segregation). Pathak et al. [4] have modeled the solidification behavior by considering the joint cause of buoyancy-driven flow and the enduring flow of the filling practice. The enduring flow influenced the development and shape of the solidification edge through the primary stages of solidification. The defects in Aluminium casting varied with the pouring rate of molten material. The pouring rate increased face defects substantially, and fewer defects appeared internally [5]. The decrease in solidification rate caused fewer pores and bigger pores, and an increase in solidification rate resulted in a finer microstructure [6]. Kakas et al. [7] discussed that porosity creation in casting is a big dilemma. These defects are minimized by altering gating system design, controlling filling at some stage, and using tolerable chills.

The casting process with various effects, i.e., turbulence flow, heat, and phase transfer, on thermal detain time was simulated with CFD by means of the solidification model in combination with the volume of fluid model. The very low heat transfer for a short time of thermal arrest produced flaws in the products. The solidification time enlarges with a highly increasing heat alternation [8]. The release of latent heat from fusion during the conversion of the liquid phase to the solid phase in casting was studied. They suggested that the proper casting design and gating system are necessary to eradicate and eliminate these defects. The faulty sites in the castings are identified by time-temperature contours in the simulation process. The shrinkage defects for casting alloys were estimated by feeding flow mode. The shrinkage imperfections are illustrated by the VOF-free surface model. The short and long freezing ranges cause internal and external shrinkage, correspondingly [9]. The vertical wall of the insertion is engaged at constant heat flux on one side and constant temperature on the other, whereas the horizontal walls are set aside as adiabatic. The applied heat transfer is a considerable parameter that controls the heat transfer and fusion velocity [10]. The casting speed and Stefan number strongly influence the thermal quality of continuous casting. The increase in Stefan number escorts to hasten the solidification process and raises the solid thickness for constant heat transfer. A decline in casting speed leads to a reduction in solid temperature. The cooling consequence of the water jacket disperses more into the central region of the molten metal inside the mold by reducing the casting speed [11]. The study was done to simulate the moving boundary with a coupled heat transfer equation and a two-phase Stefan condition. The molten flow foliage the mold quicker, and the solid thickness ingoing the secondary cooling arena is reduced with an enhances in casting speed. The numerical study of continuous casting was done with precise modeling of the flow of molten, heat transfer, solidification, and configuration of the shell by solidification and pairing [12–13]. The quality of the cast steel billet of continuous casting is affected by the cooling rate, speed of casting, and pouring temperature. Therefore, optimization of this parameter is required for suitable casting [14].

Roderick et al. [15] have done a review study on continuous casting practices for steel. They concur that the better quality of steel sheet products presents a preference for casting in the conventional continuous casting method. However, the Endless Strip Production (ESP)-Thin Slab Caster (TSC) advance is now extremely reasonable. Adan et al. [16] have simulated the heat exclusion from billets strands in the continuous casting. The model covenants with the non-symmetric cooling situations of a billet caster. The plugged nozzles are used in the secondary cooling system (SCS). The approach is adaptable as it accommodates pleasantly the changes in various casting machines, together with the use of altered types of water spray nozzles. The general heat elimination rate rises at low slab casting speeds because of longer residence times under cooling effects in the SCS. Jones et al. [17] have done a CFD simulation of vertically upward continuous casting. The oxygen-free copper casting was done at different casting speeds. The faster casting speeds created high temperatures. The increase in temperature within the die represents the occurrence of casting defects. Junde et al. [18] have studied the behavior of primary solidification and heat transfer at altered positions of the mold. The width of the total slag on the cross section is bigger at the corner than excessively at the corner. They also observed that the primary solidification and heat transfer are

considerably influenced by the width of the slag, in addition to the heat beginning from the upper backflow. Sheng et al. [19] have discussed the simulation of slab mold friction performance by varied mold turn structures in continuous casting. The liquid slag thickness diminishes step by step from the meniscus to the mold exit. The liquid slag vanishes as the temperature of the slag is lesser than its melting temperature. Chakraborty et al. [20] have studied the thermo-mechanical model of the mold with turbulent flow. In the presence of variable heat transfer, they suggested various taper profiles for the corner and the off-corner regions of the mold periphery. Further, they proposed a modified taper profile that is suitable for retaining the minimum air gap linking the billet and the mold, creating a definite process for smoothing, and demurring defects in billet casting. Huang et al. [21] have optimized residence time, homogenized the temperature, and eliminated insertions by floatation of molten metal based on the flow state of molten steel in tundish. They report that the overall velocity of the flow field, turbulent intensity, and molten steel surface velocity increase by two times the casting speed. Khadraoui et al. [22] have done the solidification modeling based on the heat equation, boundary, and initial conditions, which depend on the shape of the part, the mold, and the cooling system. They observed the solidification region on the billet axis from the temperature profiles.

Qin et al. [23] have studied a mathematical model for the flow behavior of liquid steel in the tundish. They observed some swirling flows around the stopper. The flow of liquid steel close to the liquid surface was active in the region of the stopper. By increasing the casting speed, the vortex range and intensity about the stopper regularly declines and the peak value of the vertical flow velocity of liquid steel in the locality of the stopper reduces. Sen et al. [24] have discussed the optimal temperature, velocity distribution, and turbulent intensity within the mold. Elevated turbulent intensity at the mold meniscus may also result in the trap of mold powder in steel. The lesser turbulent intensity can cause the freezing of mould powder, which may result in centre separation defects in steel. The design characteristic of SEN (sun entry of the nozzle) depends on bore diameter, bore configuration, port shape, port angle, port dimension, number of ports, and the engrossed depth of SEN within the mould. They suggested that defect-free steel can be produced through a consistent and optimized flow pattern of steel in the mold through the optimized design of SEN. Zhang et al. [25] used the standard k-turbulent model for double-stream-pouring continuous casting processing to examine the impact of the submerged entry nozzle's (SEN) depth on the velocity, temperature fields, and composition distribution in the solidification zone. They noticed that as the depth of the SEN in the mold increased, the location of the mixture of the internal and external fluids moved downward in the liquid pool. Yin et al. [26] developed a mathematical model to optimize the SEN for an ultra-thick slab mold and looked into solidification, insertion transports, and meniscus fluctuation. The convex-bottom SEN cases enhance the horizontal velocity and temperature on the meniscus while decreasing the impinging depth of the jet flow relative to concave-bottom SEN cases. The flow and solidification of molten steel are largely unaffected by the concave-bottom SEN's well depth and submerged depth. The SEN port's form and angle have a major impact on the flow of molten steel. The impinging depth of the jet flow decreases when the port form shifts from rectangle to square or as the port downward angle lowers, but the horizontal velocity and temperature on the mold-free surface are increased. The square-shaped port SEN with a downward angle was more advantageous for the ultra-thick mold.

Du et al. (27) have developed a nozzle model to examine the influences of nozzle inclination, nozzle area ratio, and side-hole aspect ratio on the fluid feature of fluid steel. The persuasion of various nozzle structures on the flow field of molten steel in the mold was mastered with this model. Auxiliary: the impact position of a thin surface, reflux area, and turbulent kinetic energy of the liquid surface were defined. The impact point of the narrow surface of the meniscus is affected by an increase in nozzle angle. The inner diameter and side-hole area of the nozzle were enlarged by the increased area ratio, which resulted in a considerable reduction in the speed of high-temperature liquid steel flowing out of the nozzle.

Further increases in the aspect ratio, the vortex center, and slight surface impact positions in the upper and lower recirculation zones primarily motivated downward and then upward, and the disparity range was mostly similar. Du et al. (28) have studied three nozzle configurations to evaluate the influence of the nozzle on the flow and solidification of steel. They also deliberated the heat transfer of fluid steel, flow field, recirculation zone, flow velocity, and free-surface turbulent kinetic energy. The fluid steel pours out from the nozzle at a definite angle. The flow rate and momentum of the fluid steel regularly decline, and two separate streams are produced once the main stream moves towards the narrow surface.

The above literature studies focused on the solidification behavior of the continuous casting process, but there were fewer studies related to the computational study of liquid flow with solidification at different temperatures, i.e., pouring temperature, inlet velocities, submerged entry nozzle, cooling jet/surrounding convective conditions, mold wall temperature, etc.

This study is done for the solidification behavior of liquid metal in a cavity during a continuous casting process with and without a jet pouring system through mathematical modeling. The governing equations are solved with a computational solidification model joined with a volume flow model. The effect of pouring velocity and temperature with a constant wall temperature is used to analyze the solidification progression by estimating the temperature, velocity, and liquid fraction profiles inside the cavity throughout solidification. The quality casting product conditions in both pouring processes are analyzed.

2 Mathematical Modeling

Solidification Model

The fluid flow problems are explained by this model during the solidification and/or melting of metals. The enthalpy-porosity formulation is used for modeling the phase change process [13, 27-29].

Energy Equation

The enthalpy (H) is deliberated by the sum of the sensible enthalpy and the latent heat of the material. Equation 1 is used as an energy equation for solidification/melting problems.

$$\frac{\partial(\rho \mathrm{H})}{\partial \mathrm{t}} + \nabla.(\rho v H) = \nabla.(k \nabla T) + S \quad (1)$$

Momentum Equation

The enthalpy-porosity processes take care of the mushy section as a porous medium. The porosity is equal to zero in fully solidified regions. Equation (2) is used to specify the momentum sink owing to the compact porosity in the mushy region.

$$\mathrm{s} = \frac{(1-\beta)^2}{(\beta^3-\varepsilon)} \mathrm{A_{mush}} (\mathrm{v} - \mathrm{v_p}) \quad (2)$$

Model of Liquid Fraction

Equation 3 is used to calculate the liquid fraction (β) as discussed by [29]:

$$\beta = \frac{\mathrm{T} - \mathrm{T_{solidus}}}{\mathrm{T_{liquidus}} - \mathrm{T_{solidus}}} \quad (3)$$

$$\text{if T less than } \mathrm{T_{solidus}}, \text{ then } \beta = 0$$
$$\text{if T more than } \mathrm{T_{solidus}}, \text{ then } \beta = 1$$

Turbulence Model

The turbulence equations are added by sinks in the mushy and solidified region to describe the occurrence of solid material [29].

$$\mathrm{s} = \frac{(1-\beta)^2}{(\beta^3+\varepsilon)} \mathrm{A_{mush}}\, \varphi \quad (4)$$

Model for Contact Resistance at Walls

The estimation of wall heat flux (q) is done by Eq. 5

$$\mathrm{q} = \frac{\mathrm{T} - \mathrm{T_w}}{(\frac{1}{\mathrm{k}} + \mathrm{R_c}(1-\beta))} \quad (5)$$

Volume of Fluid (VOF) Model

The VOF model is used for two or more immiscible fluids. In this model, a single set of momentum equations is followed by the volume fraction of each of the fluids in the province [13, 27-29]. The q_{th} fluid's volume fraction in the cell is signified as a_q and subsequent situations are specified as, If cell is vacant (of the q_{th} fluid) then a_q= 0 , If cell is filled (of the q_{th} fluid) then a_q= 1 and If cell encloses the edge between the q_{th} fluid and one or more former fluids then 0 <a_q< 1

Volume fraction Model

The following of the edge(s) between the phases are consummated by the explanation of a continuity equation for the volume fraction of one

or more of the phases. The continuity equation for q_{th} phase has the subsequent form given in Eq. 6:

$$\frac{1}{\rho_q}\left[\frac{\partial}{\partial t}\left(a_q\rho_q\right) + \nabla.\left(a_q\rho_q v_q\right) = s_{a_q} + \sum_{p=1}^{n}(m_{pq} - m_{qp})\right] \quad (6)$$

Momentum Equation

The momentum equation is reliant on the volume fractions of all phases through the properties (density (ρ) and viscosity (μ)) given in Eq. 7,

$$\frac{\partial}{\partial t}(\rho v) + \nabla.(\rho v v) = -\nabla P + \nabla[\mu(\nabla v + \nabla v^T)] + \rho g + F \quad (7)$$

Energy Equation

The energy equation given in Eq. 8, also shared along with the phases.

$$\frac{\partial}{\partial t}(\rho E) + \nabla.\left(v\,(\rho E + P)\right) = \nabla.(k_{eff}\nabla T) + S_h \quad (8)$$

3 Numerical Simulations

The governing equations, along with the former modeling equations, have been computed using a computational solidification/melting model of ANSYS (Version 19R3). The liquid zone and variable space grid methods for solidified shells are front-fixing or Boundary Immobilization Method (BIM). The heat of solidification should be taken into consideration when setting up the energy balance. There is no alteration of volume during solidification, as it is supposed that the physical properties of the material remain constant throughout the process. The variable space grid method (VSG) is used as the solidified shell thickness is varying continuously in this region. The solutions for moving boundary problems are obtained through finite difference methods. The implicit method is used to solve the resulting matrix. The convergence criteria for all variables (i.e., mass, velocities, and turbulence extents) are set as the standardized and general residue value, which is equal to 10^{-5}.

The steel as a material is used for solidification, and the thermophysical properties and input parameters of the slab caster are given in Tables 1 and 2, respectively. The geometry used in this study is a square cross-section of rectangular steel billet, as stated in Table 2. The liquid metal enters through the inlet of the mold shown in Figure 1 (a).

Table 1 Properties of steel [11]

Thermophysical properties	**Solid** **Liquid**
c (J/ kg^{o}C)	430 825
ρ (kg/ m^3)	7400 7400
k (W/ m^{o}C)	33 39
Liquids Temperature (K)	1723
Solidus Temperature (K)	1698
L_f (J kg^{-1})	260000
T_{in} (K)	1803
Solid wall temperature (K)	1118.35
Ste	1

Table 2 Geometry of the rectangular billet [11]

Section Size (mm x mm)	280mm x 280mm
Length H (mm)	670
Inlet velocity v (m/s)	0.0125
d (mm)	2
k (W m^{-1}^{o}C^{-1})	315

The simulation is done for the grid independence test and the validation of the model at the following boundary conditions that were specified by Moghada and Hosseinzadeh [11]: The pouring velocity at the inlet of the mold is 0.0125 m/s on the wall. The no-slip condition is defined, and the outlet of billet and solid wall temperature is 1118.35 K. The meshed geometry without jet is shown in Fig. 1 (b). The geometry and mesh of the billet cavity with a jet size of 140 mm are given in Figs. 1(c) and 1(d), respectively.

The grid independence test is done as per the above-specified conditions. The temperature variation for solidified shell with different grid sizes (38.0 mm, 40.0 mm, 42.0 mm, and 44.0 mm) along the normal axis from the center of the mold is shown in Fig. 2 (a). The minimum variation in temperature is observed at 42 mm grid size along the normal to the axis from the center of the mold. Therefore, the validation of the model was done for the 42-mm grid with the same conditions as those specified by Moghada and Hosseinzadeh [11] and given in Fig. 2(b). At the center, about 100 °C and

100 mm (outer surface) away from the center, less than a 50 °C temperature difference is observed. However, the behavior of temperature differences is similar to the work of Moghada and Hosseinzadeh [11]. Hence, the model is validated, and further study was done at a 42 mm grid size for 2000 second-time steps.

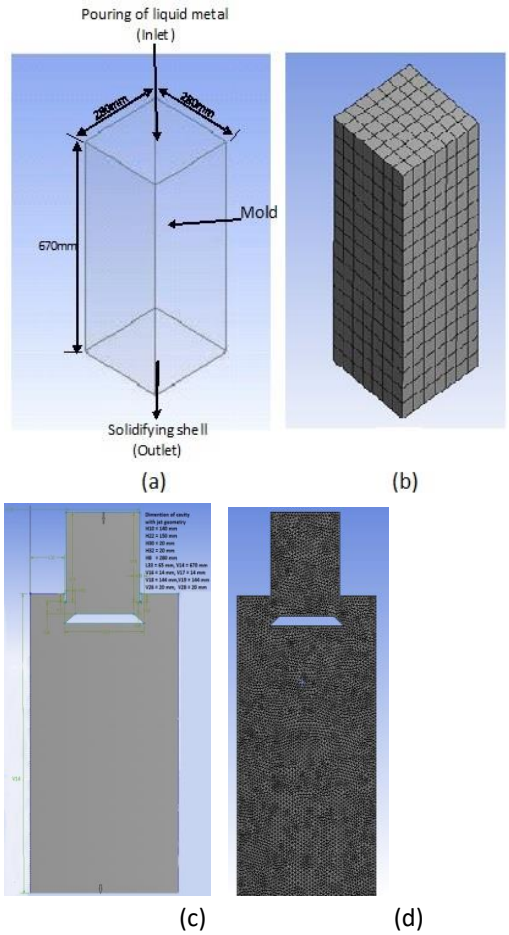

Fig. 1 Schematic of continuous casting of rectangular billet (a) geometry without jet (dimension in mm) (b) meshed geometry without jet (c) geometry with jet (dimension in mm) (d) meshed geometry with jet

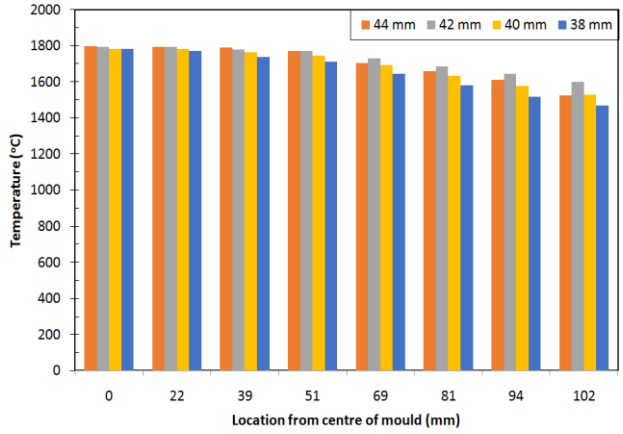

(a)

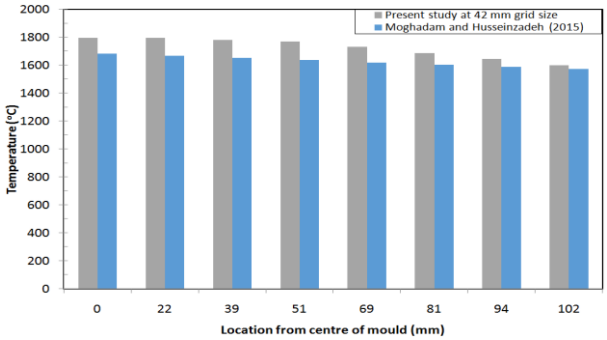

(b)

Fig. 2 Temperature variations along the normal to axis from the centre of the mold at Ste=1, casting speed 0.0125 m/s, and time step 2000 s for (a) different grids and (b) the present study at grid sizes 42 mm [11].

4 Results and Discussion

4.1 Solidification behavior without jet pouring

This section is used to discuss the cause of inlet velocity (pouring velocity) on solidification in the continuous casting process. The temperature contour for different pouring temperatures with varying inlet velocity at a constant time (2000 sec.) and the same solid wall temperature of 1118.35 K is given in Figs. 3, 4, and 5.

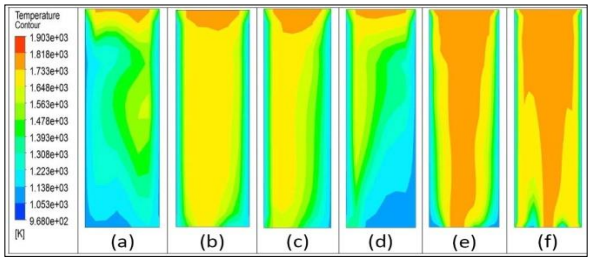

Fig. 3 Temperature variation for velocities (m/s) (a) 0.0075, (b) 0.010, (c) 0.0125, (d) 0.015, (e) 0.0175 (f) 0.02 m/s at pouring temperature 1753 K

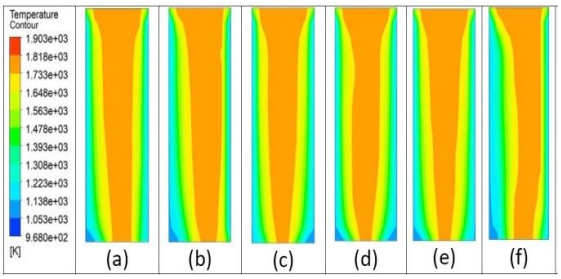

Fig. 4 Temperature variation for velocities (m/s) (a) 0.0075, (b) 0.010, (c) 0.0125, (d) 0.015[1], (e) 0.0175 (f) 0.02 m/s at pouring temperature 1803 K

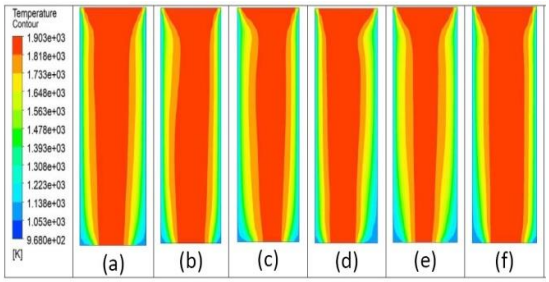

Fig. 5 Temperature variation for velocities (m/s) (a) 0.0075, (b) 0.010, (c) 0.0125, (d) 0.015, (e) 0.0175 (f) 0.02 m/s at pouring temperature 1853 K

Figure 3 shows the temperature profile at different inlet velocities at 2000 seconds for a 1753 K pouring temperature. As velocity increased from 0.0075 m/s to 0.0175 m/s, the informality in temperature distribution increases and better contour is observed at 0.0175 m/s With a further increase in velocity up to 0.02 m/s, the uniformity in temperature distribution is decreased. It was observed because solidification propagation was affected by the flow velocity. Further, as the pouring temperature increased from 1753 K to 1853 K, the temperature inside the mold increased and the region of solidification decreased; however, the temperature distribution was more uniform at all poring temperatures than at 1753 K at all inlet velocities, as shown in Figs. 3, 4, and 5. The more uniform profile is achieved at a velocity of 0.0175 m/s at 1803 K, as given in Fig. 4, with a higher solidified region. At lower velocity, the profile is not uniform, which increases the chances of defects in the casting. The higher region of liquid inside the mold at a higher temperature in Fig. 5 is caused by the inclusion of air and further creates the defect in the casting. The liquid metal near the mold walls solidifies faster than in the center part because a constant mold wall temperature of 1118.35 K is maintained in the continuous casting process through water cooling.

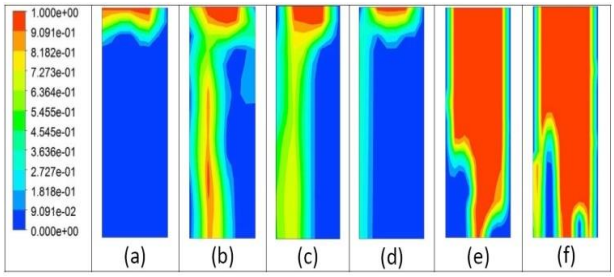

Figure 6(a). Alloy Liquid Fraction variation for velocities (m/s) (a) 0.0075, (b) 0.010, (c) 0.0125, (d) 0.015, (e) 0.0175 (f) 0.02 m/s at pouring temperature 1753 K

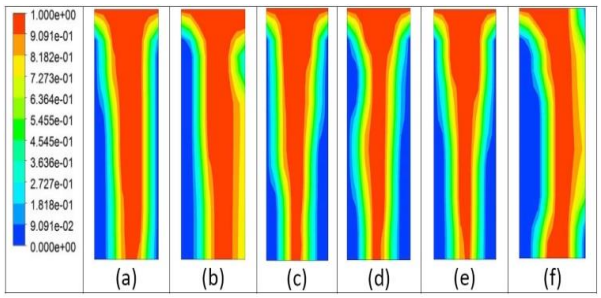

Figure 6(b). Alloy Liquid Fraction variation for velocities (m/s) (a) 0.0075, (b) 0.010, (c) 0.0125, (d) 0.015, (e) 0.0175 (f) 0.02 m/s at pouring temperature 1803 K

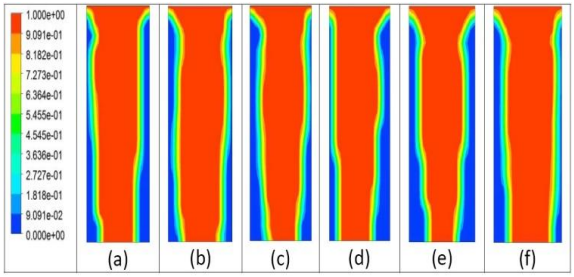

Figure 6(c). Alloy Liquid Fraction variation for velocities (m/s) (a) 0.0075, (b) 0.010, (c) 0.0125, (d) 0.015 (e) 0.0175 (f) 0.02 m/s at pouring temperature 1853 K .

The alloy liquid fraction of the mold cavity without jet pouring is shown in Fig. 6 for the same time duration (2000 sec). The solidification in the first configuration (as in Fig. 6 (a)) uniformly proceeds toward the center for increasing velocity, while the same behavior of the alloy liquid fraction is obtained for the second configuration (as in Fig. 6 (b)). But comparatively, the first configuration (Fig. 6(a)) provides better results for the same conditions. Further increasing the pouring temperature up to 1853 K, as shown in Fig. 6(c), a

larger liquid region is observed at all pouring velocities; however, at 0.0175 m/s pouring velocities, the alloy liquid fraction profile is more uniform than at other velocities. Similar behavior is also observed in the temperature profiles in Figures 3, 4, and 5. As per the uniform liquid fraction and temperature profile for different pouring temperatures (1753 K, 1803 K, and 1853 K), the pouring velocity of 0.0175 and the pouring temperature of 1803 K are the best options for a better casting product. Further, the velocity profile inside the cavity at constant pouring velocity of 0.0175 m/s for different pouring temperatures is also analyzed for better casting, as shown in Fig. 7

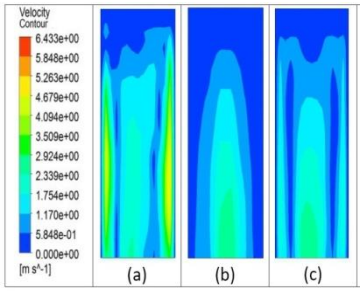

Fig. 7 Velocity variation for pouring temperature (a) 1753 K (b) 1803 K (c) 1853 K at pouring velocity 0.0175 m/s

Figures 7(a), 7(b), and 7(c) show the velocity variation inside the mold. At 0.0175 velocity, the variable pouring temperature ranges from 1753 K to 1853 K. The higher the temperature from 1753 K to 1853 K, the more uniform the velocity contour observed at the pouring temperature of 1803 K for inlet velocities of 0.0175 m/s, as shown in Fig. 7(b). This is because of the uniform temperature distribution and alloy liquid fraction inside the mold, as discussed in Figs. 3–5 and Fig. 6, respectively. The non-uniform nature of the velocity profile causes defects in the casting. The higher temperature region supports the uniform velocity but requires more time for the solicitation, which promotes gas inclusion and causes defects in the casting. Therefore, the uniform velocity profile at a pouring temperature of 1803 K for inlet velocities of 0.0175 m/s is more suitable.

4.2 Solidification behavior with jet pouring

In Section 4.1, metal liquid is directly poured at the inlet of the cavity. As per the observation, the better casting product without a jet system is found at a pouring velocity of 0.0175 m/s and a pouring temperature of 1803 K. Further study was done by using the jet for pouring the liquid metal at the center of the inlet of the cavity with a 140-mm diameter, as shown in Fig. 1(c). The temperature variation inside the cavity at different pouring velocities (0.089 to 0.218 m/s) and constant pouring temperatures (1803 K) is shown in Fig. 9. The initial velocity of 0.089 m/s in a jet pouring system is higher than the 0.0175 m/s of a non-jet system because the flow of liquid metal is divided into two streams, and a velocity of 0.0175 m/s is not sufficient to process the liquid to flow uniformly from both sides of the jet to the cavity. Even at a 0.089 m/s velocity, the flow is processable but not uniform, as shown in Fig. 8 (a) of the temperature contour.

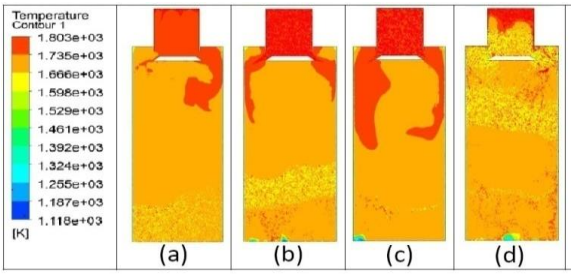

Fig. 9 8 Temperature variation for pouring velocities (m/s) (a) 0.089, (b) 0.132, (c) 0.175, (d) 0.218 m/s at pouring temperature 1803 K and jet diameter 140 mm

Further increasing the velocity from 0.089 to 0.175 m/s, the uniform temperature variation inside the cavity is observed, as shown in Fig. 8(a) to 8(c), and further increasing the velocity up to 0.218 m/s. The higher temperature is observed at the top of the jet, and the uniform distribution of temperature is disturbed because of the high velocity given in Fig. 8(d). Therefore, 0.175 m/s velocity is suitable for better casting products.

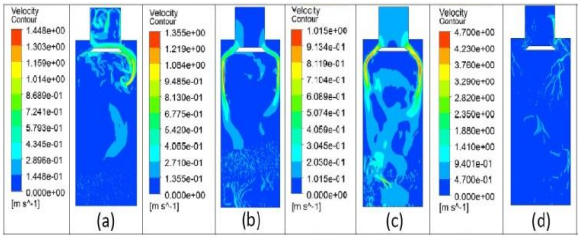

Fig. 10 9 Velocity variation for pouring velocities (m/s) (a) 0.089, (b) 0.132, (c) 0.175, (d) 0.218 at pouring temperature 1803 K and jet diameter 140 mm

The flow behaviors of liquid metal inside the cavity are analyzed by velocity variation inside the cavity at different pouring velocities at a constant pouring

temperature of 1803 K, as given in Fig. 9. The velocity profile inside the cavity at a pouring velocity of 0.089 m/s in Fig. 9 (a) shows a higher velocity at the right side of the jet and a lower velocity at the left side of the jet. Therefore, the pouring velocity of 0.089 m/s is not sufficient to process the liquid metal inside the cavity uniformly. A further increase in the pouring velocity up to 0.175 m/s uniform velocity profile is observed, as shown in Fig. 9 (b) and (c). Similar behavior is reported by Du et al. (27) and Du et al. (28). At 0.218 m/s pouring velocity, low velocity with no uniform distribution is found because of the higher velocity of the jet. A similar behavior is observed, as discussed in Fig. 8 of the temperature contour.

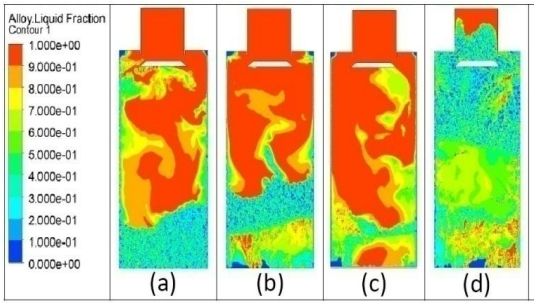

Fig. 11 10 Alloy Liquid Fraction variation for pouring velocities (m/s) (a) 0.089, (b) 0.132, (c) 0.175, (d) 0.218 at pouring temperature 1803 K and jet diameter 140 mm

The allow liquid fraction variation inside the cavity is also analyzed to understand the solidification process. The variations in allow liquid fraction for different pouring velocities are given in Fig. 10. The major solidification initiation starts at the bottom of the cavity in the jet pouring system, as shown in Fig. 10, while without jet solidification, it is initiated from the side of the cavity, and a liquid region is observed in the middle of the cavity. The possibility of the incomplete solidified product going outside the cavity is discussed in Fig. 6. Therefore, a jet pouring system is advantageous, and a better casting product can be achieved. Further, as the pouring velocity increases, a larger liquid region is observed inside the cavity with uniform variation, as shown in Figs. 10 (b) and 10 (c), and at a high pouring velocity of 0.218 m/s, a lower liquid region with a non-uniform distribution is observed because of the higher rate of removal of the product from the cavity. Therefore, the 0.175 m/s velocity is better for quality cast product in the jet pouring system, and it is 10 times higher than the without-jet quality product system at 1803 K pouring temperature.

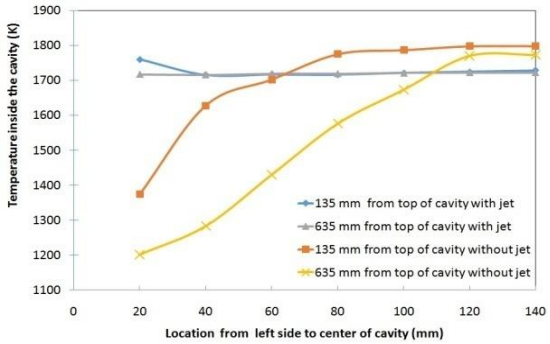

Fig. 11 Temperature variation inside the cavity at different location from left wall to centre for (a) with jet pouring velocity 0.175 m/s (b) without jet pouring 0.0175 m/s at pouring temperature 1803 K

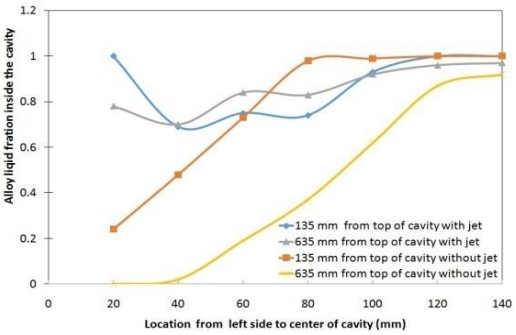

Fig. 12 Alloy Liquid fraction variation inside the cavity at different location from left wall to centre for (a) with jet pouring velocity 0.175 m/s (b) without jet pouring 0.0175 m/s at pouring temperature 1803 K

The variation of temperature inside the mold cavity at different locations with and without a jet is given in Fig. 11. The small change in temperature (50 K) is found at the left corner for 135 mm and 635 mm from the top of the cavity for the jet system, while the temperature is approximately the same in the center regions. This is because liquid metal is fed from the corner side and informs the distribution of liquid temperature inside the cavity. However, without the jet system, about a 600 K change in temperature is observed from the left side to the center of the cavity. Further temperature is varied from 200 K to 10 K from the left wall to the center of the cavity, and from the top of the cavity, 135 mm to 635 mm. At the center region temperature of 75 K, a higher temperature is found in the jet system. Similar behaviors are also observed in the alloy liquid fraction variation in Fig. 12. In view of the above fact, quality casting is found in the jet

type casting system than without the jet because more uniform temperature, liquid fraction, and velocity distribution are observed in the jet system.

5 Conclusions

This paper focused on a numerical simulation of the continuous casting process of a rectangular square cross-section steel billet. The solidification behavior is examined by estimating the temperature, velocity, and liquid fraction inside the mold for the pouring temperature (1753 K to 1853 K) and different inlet velocities with and without the jet pouring system. The investigation of the solidification process is carried out by means of av_p solidification/melting model tied to the volume of fluid. The simulation was done with the computational package ANSYS (Version 19R3).

- The uniform temperature and velocity distribution inside the mold without a jet system are observed at 1803 K pouring temperature and 0.0175 m/s velocity.
- The uniform velocity and temperature profiles suggested better propagation of solidification, which was analyzed by the alloy liquid fraction profile.
- The temperature distribution inside the cavity with the jet system is different from that without the jet system. The higher temperature region is observed at the wall of the cavity, and solidification is initiated from the bottom of the cavity while without a jet from the side wall of the cavity.
- The uniform temperature and velocity profile are observed at 1803 K pouring temperature and 0.175 m/s pouring velocity. The pouring velocity is 10 times higher than without a jet system.

Nomenclatures

A_{mush} Mushy zone constant
B Liquid volume fraction
C_p Specific heat at constant pressure.
E Energy
E_p Every phase is based on the specific heat of that
phase
F External body force.
H Enthalpy
h_{ref} Reference enthalpy
k Thermal conductivity
k_{eff} Effective thermal conductivity.
l Distance between the wall and the location
L Latent heat of material.
m_{pq} mass transfer from phase p to phase q
m_{qp} Mass transfer from phase q to phase p
P Static pressure
Rc Contact resistance
S Source term
S_h Heat source
T Temperature at location within the cell
T_{ref} Reference temperature,
T_w Temperature of wall
v Fluid velocity
Solid velocity because of the pulling of solidified material out of the domain
ρ Density
ε Small number (0.001) to avoid division by zero
φ Turbulence parameter

References

[1] Im, I.T., Kim, W.S., Lee, K.S. (2001), "A unified analysis of filling and solidification in casting with natural convection", Int. J. Heat and Mass Transfer, Vol. 44, pp. 1507-1515.

[2] Swaminathan, C.R., Voller, V.R. (1992), "A general enthalpy method for modeling solidification process", Metall Trans., Vol. 23(B), pp. 651-664.

[3] Swaminathan, C.R., Voller, V.R. (1994), "A time-implicit filling algorithm", Appl. Appl. Math. Modelling, Vol. 18, pp. 101-108.

[4] Pathak, N., Kumar, A., Yadav, A., Dutta, P.(2009) "Effects of mould filling on evolution of the solid–liquid interface during solidification", Appl. Thermal Engineering, Vol. 29, pp. 3669–3678.

[5] Jadayil, W.M. (2011), "Studying the effects of varying the pouring rate on the casting defects using non-destructive testing techniques" Jor. J. Mechanical and Industrial Engineering, Vol. 5, pp. 521-526.

[6] Vander, B.D. (2005), "Effects of solidification rate on porosity formation and cast microstructure in aluminum alloy a356. laboratory module 3 EGR 250" Materials Science & Engineering (2005).

[7] Kakas, D., Kovacevic, L., Pal, T. (2008), "Improvement of casting process control by computer simulation and experimental

observation", Proceedings of the 3rd International Conference on Manufacturing Engineering, Greece (2008).

[8] Nguyen, D.K., Huang, S.C. (2012), "Analysis the effects of turbulence flow, the heat, and phases transfer on thermal arrest time in casting process by computational fluid dynamic method", J. Eng. Tech. and Education, Vol. 9, pp. 436-450.

[9] Reis, A., Houbaert, Y., Xu, Z ., Van, T.R., Santos, A.D., Duarte, J.F., Magalhaes, A.B. (2008), "Modeling of shrinkage defects during solidification of long and short freezing materials", Journal Mat. Proc. Tech. Vol. 202, pp. 428–434.

[10] Mbaye, M ., Bilgen, E. (2001), "Phase change process by natural convection-diffusion in rectangular enclosures", Heat and Mass Transfer , Vol. 37, pp. 35-42

[11] Moghadam, A.J., Hosseinzadeh, H. (2015), "Thermal simulation of solidification process in continuous casting", Int. J. Engineering, Vol. 28 No. 5 , pp. 812-821.

[12] Thomas, B.G. (2001), "Continuous casting", The Encyclopedia of Mate: Sci. and Tech, K.H. J. Buschow, R. Cahn, M. Flemings, B. Ilschner, E. J. Kramer, S. Mahajan, (D. Apelian, subject ed.) Elsevier Science Ltd., Oxford, UK., Vol. 2, pp. 1595-1599.

[13] Amratav, N., Kumar, K., Pillai, M. (2021), "Computer simulation of continuous casting processes: A Review", Adva. in Materials, Vol. 10 No. 3, pp. 31-41.

[14] Khurram, M ., Iqbal, S., Fahad, A. Quddoos, S.M. (2022), "The effect of temperature, cooling rate and casting speed on quality of continuous cast steel billets", Advanced Mate. Research, Vol. 1171, pp. 61-72.

[15] Roderick, I. L., Guthrie, Roderick, M.I. (2022), "Continuous casting practices for steel: past, present and future", Metals, Vol. 12 No.862, pp. 1-12.

[16] Adán, R. L., Omar, D.M., Alfonso, N.B. Morales, R. D., Jafeth, R. A., Carlos, R. M. V. (2021), "Analysis of non-symmetrical heat removal during casting of steel billets and slabs", Metals, Vol. 11 No. 9, pp. 1380

[17] Jones, T. D. A., Strachan, R. I., Mackie, D. M., Cooper, M., B., Frame, Vorstius, B. J. B.(2021), "Computational fluid dynamic simulations of solidification for enhancing speed of continuous cast copper. Engineering Science and Technology", An International Journal, Vol. 24 No. 1, pp. 92 – 104.

[18] Junde, J., Yumin, M., Zhang, X., Chen, W., Zhang, L., Wang, Q. (2021), Initial solidification and heat transfer at different locations of slab continuous casting mold through 3D coupled model", Steel Research International, Vol. 92 No. 7, pp. 2000714

[19] Sheng, Y., Longa, M., Chena, D., Fana, H., Yua, H., Duana, H., Xiea, X., Liua, T. (2019), "Effect of the mold corner structure on the friction behavior in slab continuous casting molds", Journal of Materials Processing Tech., Vol. 270, pp. 157-167.

[20] Chakraborty, S., Ganguly, S., Talukdara, P. (2019), "Determination of optimal taper in continuous casting billet mould using thermo-mechanical models of mould and billet", Journal of Materials Processing Tech., Vol. 270, pp.132-141

[21] Huang, J., Yuan, Z., Shi, S., Wang, B., Liu, C. (2019) "Flow characteristics for two-strand tundish in continuous slab casting using PIV", Metals, Vol. 239 No. 9, pp. 1-10.

[22] Khadraoui, Y., Korti, A. I. N., Seddini, A., Terfous, A., Ghenaim, A. (2007) "Simulation of the solidification process during continuous casting", International Journal of Applied Engineering Research, Vol. 2 No. 3, pp. 395–409

[23] Qin, X., Cheng, C., Li, Y., Zhang, C., Zhang J., Jin, Y. (2019) "A simulation study on the flow behavior of liquid steel in tundish with annular argon blowing in the upper nozzle", Metals, Vol. 9 No. 225, pp.1-16

[24] Sen, A., Prasad, B., Sahu, J. K.,Tiwari, J. N. (2015) "Designing of sub-entry nozzle for casting defect-free steel", IOP Conf. Series: Materials Science and Engineering, Vol. 75 No. 012006, pp. 1-6.

[25] Zhanga, W., Gao, J., Rohatgi, P. K. , Zhao, H. , Li, Y. (2009) "Effect of the depth of the submerged entry nozzle in the mold on heat", Journal of Materials Processing Technology, Vol. 209 , pp. 5536–5544.

[26] Yin, Y., Zhang, J., Xiao, P. (2023) "Mathematical modeling on optimization of submerged entry nozzle for an ultra-thick slab continuous casting mold. Metals, Vol. 13 No. 221, pp. 1-18

[27] Du, F., Li, T., Zheng, G. (2022) The effects of nozzle inclination, area ratio, and side-hole aspect ratio on the flow behavior in mold, Coatings, Vol. 12 No. 815, pp. 1-12
[28] Du, F., Li, T., Zeng, Y., Zhang, K. (2022) Influence of nozzle design on flow characteristic in the continuous casting machinery, Coatings, Vo. 12 (5) No. 631, pp. 1-11
[29] Ansys, Inc., FLUENT 19.0 R3. (2019), "User's Guide", Canonsburg, PA (2019)